The 8th International Conference
on the Application of Stress-Wave Theory to Piles,
Lisbon, Portugal, 8–10 September 2008.

J.A. Santos, Editor

isbn 978-1-58603-909-7

Keynotes

- *Goble, G.*: The use of dynamic methods in pile installation and design
- *Fellenius, B.H. & Massarsch, K.R.*: Comments on the current and future use of pile dynamic testing
- *Rausche, F., Nagy, M. & Likins, G.*: Mastering the art of pile testing
- *Middendorp, P.*: Recent developments in dynamic pile testing
- *Matsumoto, T., Matsuzawa, K. & Kitiyodom, P.*: A role of pile load test – Pile load test as element test for design of foundation system
- ***Paikowsky, S.G. & Chernauskas, L.R.*: Dynamic analysis of open-ended pipe piles**
- *Katzenbach, R., Ramm, H. & Waberseck, T.*: Economic and environment-friendly ways of designing and using deep foundations

Dynamic analysis of open-ended pipe piles

Paikowsky, S.G.
Geotechnical Engineering Research Laboratory, Department of Civil & Environmental Engineering, University of Massachusetts, Lowell, MA 01854 U.S.A.
Geosciences Testing and Research, Inc. (GTR), N. Chelmsford, MA, 01863 U.S.A.

Chernauskas, L.R.
Geosciences Testing and Research, Inc. (GTR), N. Chelmsford, MA, 01863 U.S.A.

Keywords: pile, open pipe pile, soil-plug, plugging, pile-plugging, dynamic analysis, stress-wave

ABSTRACT: An open ended pipe pile can become plugged when sufficient frictional resistance is developed by the inner soil cylinder within the pile (soil plug), thereby partially or completely preventing further intrusion of the soil into the pile. When plugging occurs in an impact driven pipe pile, a complex interaction between the pile and the soil plug takes place, causing the propagating stress wave to undergo an abrupt change. Current dynamic analyses of piles are based on the one-dimensional wave equation. Although the wave equation has the capability to indirectly (accommodate) the inner soil cylinder, it does not accurately simulate the physical phenomena when the pile is plugged, causing the predicted capacity of plugged piles based on the analyses utilizing that formulation to differ from actual field observations.

A review of the pile plugging phenomenon is presented describing its identification, plugging mechanism, and its effects on pile performance when driven in predominantly cohesive or granular subsurface. The influence of artificially plugged piles on pile resistance and performance is demonstrated via a case history. The need for correct, physical modeling of the stress wave propagation in plugged piles is established.

A different approach is investigated in which the spatial stress transformation within the soil plug is modeled using an axi-symmetric wave propagation formulation. A two-dimensional finite difference solution was developed for that formulation. This numerical solution was implemented in a computer program called PWAP (Plug Wave Analysis Program). A case study was then used to examine the applicability of the solution and to determine if the static capacity of the pile could be predicted more accurately. The PWAP analysis was performed on a pipe pile driven in Empire Clay using dynamic records taken from a well documented case study. The results of PWAP were compared to the results of programs based on one-dimensional wave equation (TEPWAP and CAPWAP), which do not simulate the effects of soil plugging. The PWAP analysis resulted in a better force match than the conventional analyses and predicted the pile capacity to 87% of the load test value, compared to about 30% for the conventional method predictions.

1 PIPE PILE PLUGGING

1.1 Overview

Pipes constitute strong and light weight structures, easy to handle and splice. Small diameter closed ended piles (typically below 18 inch, 457.2 mm O.D.) are used in land construction and are then concrete filled (cast-in-place). Large diameter piles (typically 42 to 96 inch, 1.07 to 2.44 m, in diameter) capable of carrying large axial and lateral loads are used for marine construction and for earthquake retrofitting of existing bridges and similar structures. By and large these piles are considered thin – walled piles with Outside Diameter (O.D.) to tip wall thickness (t) ratio of B/t $\approx$ 34 (Paikowsky et al. 1989). These piles are not being driven closed ended due to the difficulties associated in forcing their penetration, as well as the adverse effects of large soil displacements accompanying their insertion.

The penetration of open pipe piles into soil creates unique soil-structure interactions both inside and outside the pile. During the initial stage of installation, the soil elevation inside the pile does not change, i.e. the length of the inner soil cylinder is approximately equal to the depth of penetration depending mostly on the tip and pile geometries. The soil volume displaced under the tip is either being completely pushed out, or half pushed out and half penetrates the pile with any combination in between the two modes being possible. The pile is penetrating at that stage in a ''cookie-cutter'' mode and is considered to be unplugged (Fig. 1a). As penetration continues, the inner soil cylinder develops frictional resistance which may prevent some of the soil ahead of the opening from entering

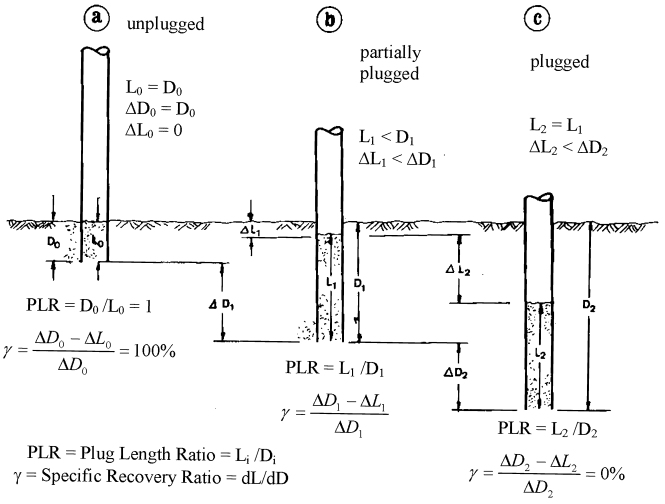

Figure 1. Three possible states of the inner soil: (a) unplugged – free soil intrusion, (b) partially plugged – limited soil intrusion, and (c) fully plugged – no soil intrusion.

the pile, i.e. the length of the inner soil cylinder is less than the penetration depth (accounting for the geometry of the pile) and the pile is considered partially plugged (see Fig. 1b). With further penetration the inner soil cylinder may develop sufficient frictional resistance to prevent most or all soil intrusion, causing the pile to become ''plugged''. The open-ended pile then assumes the penetration characteristics of a closed-ended pile.

1.2 Plugging identification

It is important to note that full plugging can take place after a significant depth of unplugged or partially plugged mode of penetration. As such, plugging is better identified using a specific recovery ratio; γ (Paikowsky et al., 1989)

$$\gamma = \frac{dL}{dD} \approx \left(\frac{\Delta L}{\Delta D}\right) \times 100\% \qquad (1)$$

ΔL = incremental plug length
ΔD = incremental pile penetration

Such that $\gamma = 0$ refers to complete plugging and $\gamma = 100\%$ refers to unplugged penetration.

Fig. 2 presents a plugging analysis of 48 inch (1.22 m) O.D. piles driven in the Gulf of Mexico presented by Paikowsky et al. (1989). The data in Fig. 2 indicate that plugging took place for all piles at a penetration depth in excess of 300 ft (91.4 m) (D/B $\geq$ 75). Due to lack of continuous plugging measurement data, the actual penetration mode of the piles at a depth greater than 300 ft (91.4 m) is not known but can be speculated to be either in a steady partial plugging mode (as illustrated by the lines in Fig. 2) or in a cookie cutter mode to a depth of 375 ft (114.3 m), followed by penetration in a completely plugged mode for about 45 ft (13.7 m). Fig. 3 shows the driving record of a typical pile at this site where at a penetration depth of 300 ft (91.4 m) an 8 hour break for

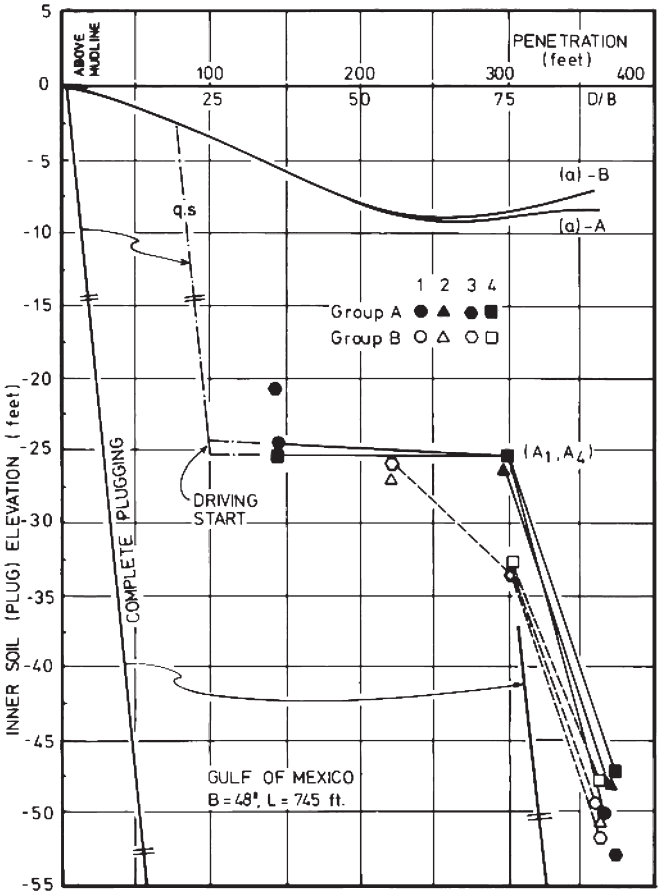

Figure 2. Analysis of plugging measurements for B = 48 inch (1.22 m) O.D. piles in the Gulf of Mexico.

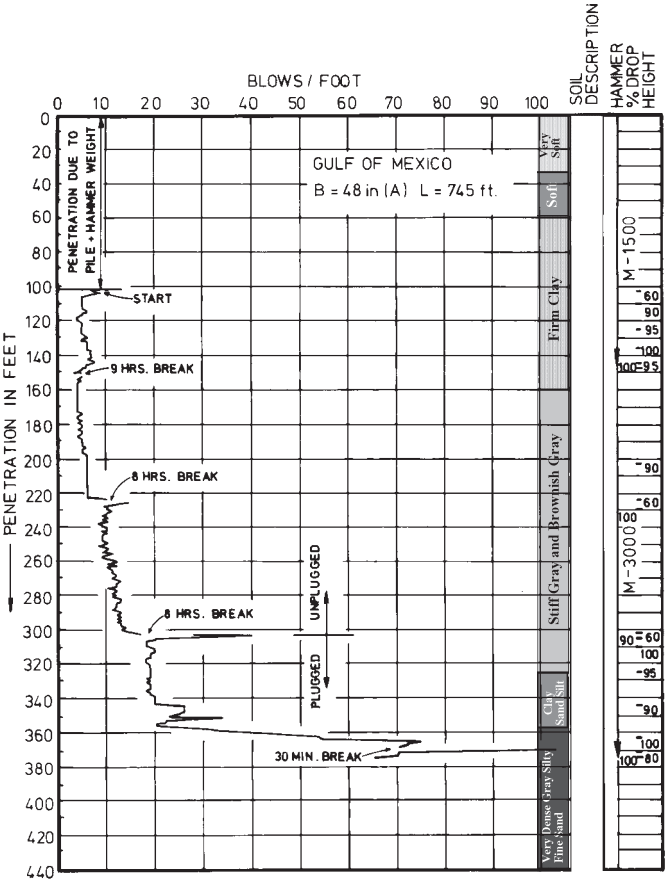

Figure 3. Driving record of diameter B = 48 inch (1.22 m) pile in the Gulf of Mexico.

an add-on section resulted in a very high driving resistance upon the resumption of driving. The following penetration resistance (expressed by the number of blows per foot of penetration N) exhibits a slight change due to plug formation. However, in view of other factors contributing to change in N (at least in clay), the detection of plugging by driving resistance is not feasible once the pore pressure is built up following a short distance of pile penetration. A separate analysis (not presented here) conducted for the pile resistance in the sand (depth of about 360 ft, 109.7 m) showed that the resistance in the sand can be explained only by the fact that the pile was already plugged as it encountered the sand.

Although technically the inner soil can be referred to as a "plug" only when it prevents entry of additional soil during penetration, the term "soil plug" is commonly used in reference to any soil mass inside the pile, regardless of its state during installation.

The complex pile-soil interaction includes: (i) transfer in mechanism from a cookie-cutter to a plugged mode and (ii) pile response both under static and dynamic loads. A comprehensive attempt to address the problem is unrealistic. The different aspects of the problem are discussed below, expanding upon the stress-wave problem and problem formulation during the "plugged" condition.

2 PILE-PLUG PROBLEM IN CLAY

Paikowsky and Whitman (1990) reviewed the effect of pile plugging on pile performance and design. They demonstrated that the contribution of the tip resistance to the total capacity for piles in clay is small (10 to 20%) considering typical pile penetrations (depth (D) over diameter (B) $D/B \geq 50$). Plugging in low permeability soils, therefore, mostly affects the soil volume displaced around the pile and, hence, the time for pore water pressure dissipation and pile capacity gain.

Fig. 4 presents predicted pore pressure dissipation decay around plugged and unplugged piles based on probe (PLS) field measurements in Boston Blue Clay (BBC). The normalization process used in developing Fig. 4 assumes that the pore pressure dissipation time is controlled by radial consolidation and, hence, is a function of the displaced soil volume. As such, for closed-ended piles, the ratio of dissipation time of one pile (t_1) with diameter R_1 in relation to another pile (t_2, R_2) is:

$$\frac{t_1}{t_2} = \left(\frac{R_1}{R_2}\right)^2 \tag{2}$$

These relationships were validated by a large database as shown in Fig. 5. The extrapolation of these relations to open and closed ended piles can be simplified by using the relations:

$$\frac{t_1}{t_2} = \frac{R_0^2}{R_0^2 - R_i^2} \tag{3}$$

For which R_0 is the outer radius of the piles (B/2) and R_i is the inner radius of the open ended pile (R_0–t). For a more comprehensive solution, see for example Carter et al. (1979).

The data in Fig. 4 suggest that when a 48 in. O.D. pile is plugged (i.e. closed ended), the time for pore water pressure dissipation to about 20% level of initial pore pressure is about five (5) times that of a pile driven unplugged.

Fig. 6 presents a pile capacity gain with time related to the open and closed ended piles referred to in Fig. 4. The figure also presents data of capacity gain with time from measurements. Further details about the issue are presented by Paikowsky et al. (1995), Paikowsky and Hart (2000), and Paikowsky and Hajduk (2006). The

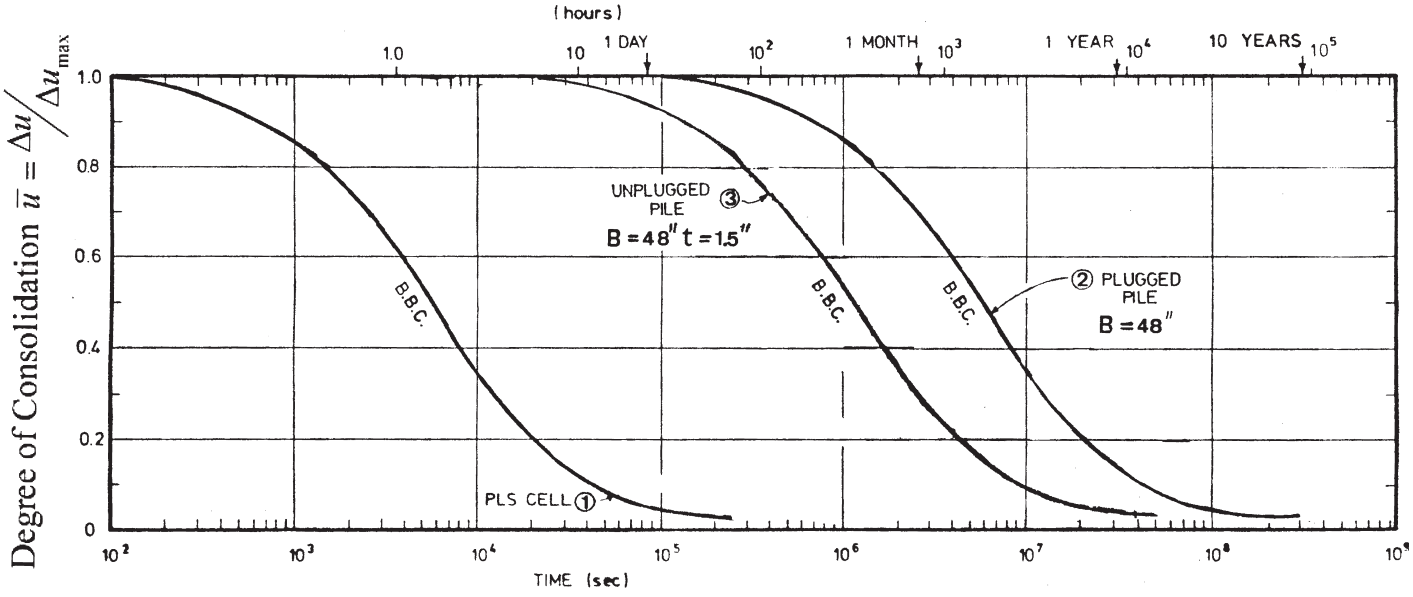

Figure 4. Predicted pore pressure dissipation decay around plugged and unplugged piles (based on PLS measurements) (Paikowsky and Whitman, 1990).

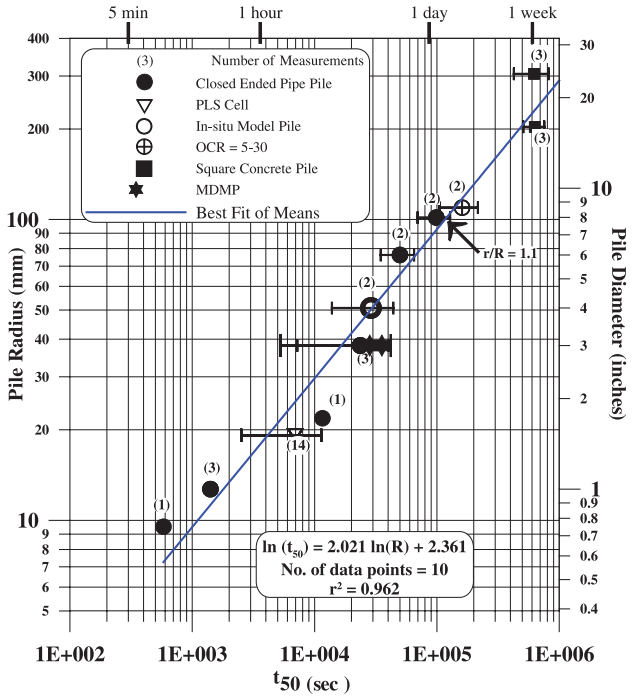

Figure 5. Effect of pile radius on t_{50} (time for 50% excess pore pressure dissipation) for NC clays (OCR = 1–2), including MDMP data (based on Paikowsky et al., 1995; see also Paikowsky and Hart, 2000).

conclusions derived are that pile plugging in clay changes the mode of pile penetration by which fully plugged penetration results with a lengthy period of pore pressure dissipation and capacity gain when compared to unplugged penetration mode.

From a dynamic pile analysis point of view, an accurate interpretation of dynamic measurements during a pile's restrike over time becomes, therefore, a most important necessity when evaluating pile capacity. Such interpretation requires a physically correct soil plug – pile formulation and simulation,hence, becoming mostly a dynamic wave-propagation problem, to be further discussed in this paper.

3 PILE-PLUG PROBLEM IN SAND

3.1 Significance and mechanism

In contrast to piles in clay, the contribution of the tip resistance to the total pile capacity in sand is quite significant; 30 to 40% when considering typical pile penetration of D/B ≈ 50. When referring to large diameter piles for which often D/B < 50, the tip contribution of plugged or closed ended piles can easily exceed 50% of the total pile capacity. Due to the difference in the failure mechanisms between the friction resistance along the pile and the end bearing, the overall contribution of the tip resistance for piles in granular soils increases with the pile's displacement and provides additional safety via its strain hardening process. These differences are of great significance when considering the failure mode of open unplugged piles compared to that of plugged or closed ended piles.

Granular materials are capable of a load transfer mechanism via chain-like particle to particle contact rearrangement along the major principal stress trajectory. This preferable load-transfer micro-mechanism manifests itself in the form of arching by which a loaded soil is capable of developing high resistance while transferring the load to a less yielding zone (for basic micro mechanics principles see, for example, Tien and Paikowsky (2001), Paikowsky and Tien (2002), and Paikowsky et al. (2003)). The development and destruction of arches in the opening of pipe piles penetrating in granular soil was postulated and analyzed by Paikowsky (1989) as presented in Fig. 7 (Paikowsky, 1990).

3.2 Stress conditions in the soil plug

Two possible relative soil/wall movements can take place: (i) 'Active' (associated with ''active arching''),

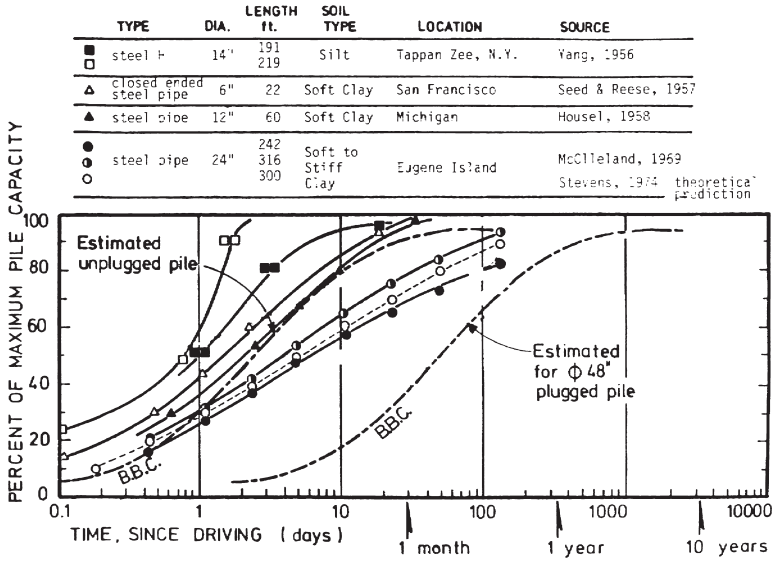

Figure 6. Comparison between predicted set up time for a 48 inch pile with field data collected by Vesić, 1977 (Paikowsky and Whitman, 1990).

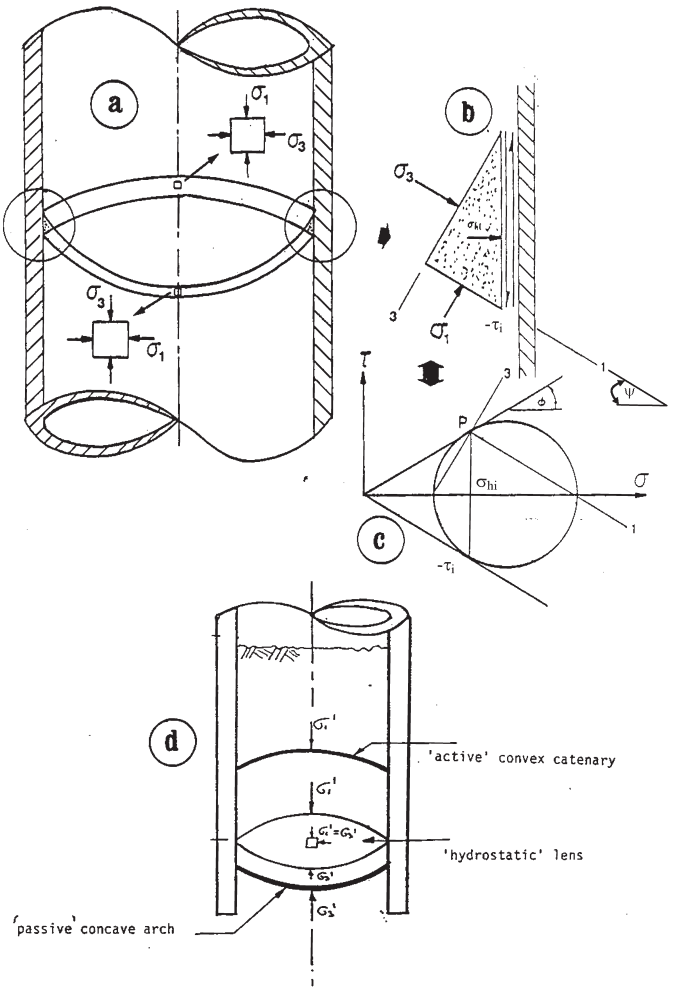

Figure 7. The state of stress in the soil plug (a) possible principal stress trajectories, (b) free body diagram, (c) Mohr Circle for the state of stress along the interface, and (d) the transition from 'active' to 'passive' arching (Paikowsky, 1990).

in which the soil settles in respect to the walls, e.g. silo or soil between retaining walls; (ii) 'Passive', in which the walls move downward with respect to the soil (or the soil is pushed upward), e.g. open pile penetration.

Two possible continuous arch trajectories for the principal stresses are presented in Fig. 7a. The stresses acting on the soil and pile interface elements are described by the free body diagram in Fig. 7b.

In penetration or static loading, the pile moves downward with respect to the soil. The shear stresses are therefore acting downward on the soil and upward on the pile. Mohr circle description of the state of stresses at a point along the interface is shown in Fig. 7c. Knowing the shear stress direction at the interface, and assuming (for the demonstration only) a 'rough' surface along this plane ($\delta = \phi$), the directions of the principal stresses at the interface are identified with the help of the pole (P). These directions lead to the two possible stress trajectories of Fig. 7a. Assuming a vertical direction for the major principal stress along the center line of the pipe, the trajectory of the minor principal stress is then convex (upward), similar to solutions which can be obtained using elasticity or plasticity theories. When the major principal stress along the center line is assumed to be in the horizontal direction, the trajectory of the major principal stress is concave (downward).

Upward shear stresses act on the soil in the 'active' arching condition, resulting in a convex major principal stress trajectory (identical to the minor principal stress trajectory of Fig. 7a). Based on the micro-behavior of granular material, it is assumed that a 'path' of contacts will be created in this direction, 'supporting' the load above it. This is actually the same mechanism which develops in silos, where the gravitational flow is downward.

In the condition of pile plugging, the soil is being pushed upward in a 'passive arching' mode, in which a supporting arch made of grain contacts is oriented concavely (downward), in the major principal stress direction as shown in Fig. 7. This observation is supported by the arch shapes formed in an overdriven sampler or in the cone-shape soil developing under closed-ended piles (for details see Paikowsky, 1990).

Both possible trajectories of Fig. 7a satisfy the stress state at the boundaries, and they 'complement' each other. A general solution for the state of stress at the boundaries was developed by Paikowsky (1989) as a function of the arching angle, ψ (measured between the horizontal radius or the vertical center line and the plane on which the major principal stress acts), the internal friction angle, ϕ, and the interface friction angle, δ. It should be noted that the analyzed arches comprise a cross-section of a spherical cap (as the problem of the soil plug is axisymmetric), shown as a segment of a circle.

The spherical caps are bounded by surfaces representing planes of zero shearing stresses. Thus, moment equilibrium requires that the stresses be constant throughout the arch following (therefore) the shape of the trajectory.

The natural soil structure resisting the downward movement of the pile (equivalent to the upward movement of the soil) is a concave arch (downward). The formation and reformation of rupture surfaces, referred to as dynamic arching, was observed by several researchers (e.g. Perry and Handley, 1967) investigating the flow of granular material discharged from model hoppers. The formation of the arch has been shown to be linked with cyclic peak stresses on the walls of the bunker accompanied by a decrease in the pressure within the soil mass, just above the dynamic arch.

The flow of soil inside the pile differs from that of the material in the silo. During discharge, the material in the silo (above the arch) undergoes very small strains (less than 1%; note that the opening of a hopper in silos is much smaller than the bin's cross-section), and moves downward in a slow motion, similar to a rigid body motion (Bransby et al., 1973). In the pile, on the other hand, it is expected that the failure of the concave arch and the continuation of the flow upward leads to reverse

shapes of convex arches. Assuming these arches are of uniform density and thickness, and thus of uniform weight throughout, the shape of the arch will be that of a catenary.

The penetration process of an open pipe-pile can be followed in Fig. 7d. At initial penetration, the circumferential friction forces are limited; the arches cannot develop the required resistance to the forces which push the soil upward, and so collapse. This situation is associated with a major principal stress along the center line (vertical) and with convex arches.

Further penetration is expected to increase the upward pushing forces only to a maximal value, corresponding to the critical depth (at which the bearing capacity stresses are maximal and do not increase more with the depth). The resisting forces, however, increase continuously with the increase in plug length, a process which is closely related to the gradual increase in the lateral stresses. At a certain plug length, the lateral confinement will bring about a special state of stress in which the 'passive' arch will not be destroyed, and the vertical stress will be equal to the horizontal stress at the interface ($K_i = 1$). This transition state is distinguished by $\psi = 45°$ with identical arches for both trajectories. It is assumed that a transition layer (with a possible lens shape) may be created, in which hydrostatic stresses will exist ($\sigma_1 = \sigma_3$).

Further build-up of stresses will enable the mobilization of the full passive arch. In this state, the soil plug mobilizes sufficient resistance to react to the upward pushing forces and to allow the lateral confinement to develop passive arches of contacts along the major principal stress trajectories. These arches may transfer horizontal stresses at the interface which are greater than the vertical stresses, associated with a horizontal major principal stress along the center line, and ψ in the range of $0° \leq \psi < 45°$ for $K_i > 1$.

The above described mechanism is translated to soil deformations inside the pile that are associated with a convex arch in the initial penetration, followed by a transition zone at the central part of the penetration. The lower densified area is a result of the passive concave arch development in the confined plug. This theory of stress and deformation conditions was demonstrated via experiments by Paikowsky (1990).

3.3 Model testing

If the mechanism described above is correct, then it can be detected through an experimental study. Because past experimental data were obtained without an understanding of the underlying mechanism, their interpretation could indicate the existence of a certain mechanism, but could not validate it.

This plugging mechanism should manifest itself through the consequences of arch formation and destruction in the following ways:

1. Beyond the initial stage of penetration, the build-up of the concave arches should be associated with an increase in the resistance to penetration, which is reduced upon arch failure and reappears upon arch reformation as penetration continues.
2. The detection of arch formation should be associated with the initiation of pile plugging.
3. The arch build-up and destruction should be expressed as variations in: (a) straining and therefore densification of the soil plug, and (b) plugging as expressed by the specific recovery ratio.

Results from tests on model piles are presented in Fig. 8. The data of Fig. 8 were obtained from the continuous penetration of a 44.5 mm ($1\,^3/_4$ inch) diameter pile with a wall thickness of 1.6 mm ($^1/_{16}$ inch) (B/t = 28) into a medium dense Ottawa sand at a constant rate of 20 mm/minute.

Fig. 8a describes the resistance to penetration (driving force) with depth from initial penetration to the final depth of 500 mm (20 inches). To a depth of

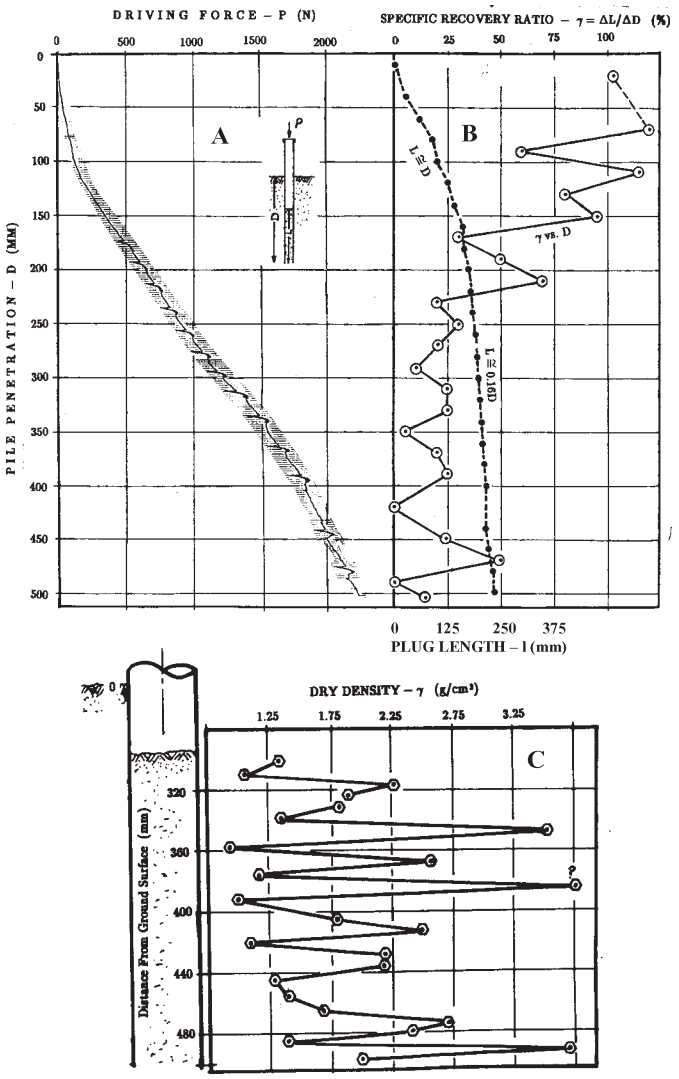

Figure 8. Model pile test results; (a) driving force vs. penetration, (b) plug length and specific recovery ratio vs. penetration, and (c) dry density distribution along the soil plug (Paikowsky, 1990).

about 177 mm, a gradual increase in the pushing force with increased penetration is observed. At 175 mm an abrupt decrease in the pushing force was recorded, while a downward movement of the inner soil mass was observed simultaneously (this could be observed through the transparent pipe and measured plug elevation). As penetration continued, abrupt reductions followed by build-up of the pushing force were detected at regular intervals of about 20 mm. The intervals seemed to increase toward the end of penetration. These force variations match the expected arch mechanism, showing a decrease in the force at each instance of arch failure, followed by a build-up as the arch re-forms.

Fig. 8b presents the relations between the inner soil length (L) and the specific recovery ratio (γ) vs. penetration depth (D). The plug length vs. penetration relations indicate that a change in the plugging occurs at a depth of approximately 170 mm, where the slope of L vs. D changes. Until that point, the plug length is approximately equal to the penetration depth ($L \cong D$). From then on, however, the plug length increases at a slower rate compared to the penetration ($L \cong 0.16D$). The depth at which this change occurs corresponds to the aforementioned first recording of force change, as shown in Fig. 8a.

The specific recovery vs. depth relations serve as a more concise indication of the plugging mechanism and the relations of Fig. 8a. Partial plugging was detected at a depth of about 90 mm, indicated by the change in the force vs. penetration relation of Fig. 8a. At 175 mm depth, a marked reduction in γ (from about 100% to 30%) coincides with the observations of the plug movement and the first abrupt change in the pushing force, indicating the build-up and destruction of the first significant concave arch. From that depth, a continuous trend of decrease in γ (recorded in spikes) reflects the increased resistance of the arches to the penetrating soil. As an arch forms, soil penetration is prevented and γ decreases; upon arch failure, soil penetrates and γ increases. However, since the plug length measurements were recorded at 20 mm intervals (during penetration), their accuracy in detecting the process is limited; even though the changes in γ correlate well with the measured changes in force shown in Fig. 8a.

Fig. 8c presents the changes in density inside the 228 mm long soil plug at the end of penetration. The dry density at the top of the plug ($\gamma \approx 1.18$ g/cm^3) is less than the initial soil density ($\gamma_i = 1.74$ g/cm^3). The average density increases from approximately 1.54 g/cm^3 at the upper 48 mm to 1.99 g/cm^3 at the lower 48 mm. The detailed density measurements enable the variations of the soil density in the plug to be tracked and provide additional support to the proposed mechanism. Layers of densified soil due to compaction of stress build-up are followed by loose soil layers as a result of arch failure and reentrance of sand. This is in good agreement with the force and specific recovery ratio variations with depth shown in Figs. 8a and 8b.

While the pseudo static analysis of the phenomenon is possible, its formulation and analyses under transient dynamic forces during impact are more complex. The response of the plugged pile to a stress wave remains a problem beyond the fundamental mechanism that governs the granular material-pile interaction and will be addressed below in a general formulation.

4 OPEN PIPE PILE BEHAVIOR UNDER A STRESS-WAVE

4.1 General theory

To understand the basic problem associated with dynamically analyzing plugged piles by conventional Wave Equation (WE) analysis, the fundamental theory must be presented. An impact on an elastic, isotropic, homogenous body results with stress propagation from the point of impact in a three dimensional fashion. These waves, when assuming that the motion includes change in shape and translation (but not rotation), conveniently formulate into a Cartesian axis presentation for waves of dilation (compression) and distortion (equi-voluminal – shear waves) in the following way (Timoshenko and Goodier, 1970; Graff, 1975):

$$\frac{\partial^2 \psi}{\partial t^2} = c^2 \nabla^2 \psi \tag{4}$$

in which:

ψ(u,v,w) where u, v, and w are movements in directions x, y, and z, respectively
∇^2 = Laplacian = $\partial^2/\partial x^2 + \partial^2/\partial y^2 + \partial^2/\partial z^2$
for compressive wave $c = c_1 = \sqrt{\lambda + 2G/\rho}$
for distortion wave $c = c_2 = \sqrt{G/\rho}$
ρ – mass density,
G – shear modulus,
ν – Poisson's ratio,
E – modulus of elasticity

$$\lambda = \frac{vE}{(1+v)(1-2v)}$$

The general propagation of waves in elastic media is comprised of the combination of the above two wave types together.

The above presentation is often forgotten when applying stress wave theory to piles because the one dimensional wave equation (1-D W.E.) has been employed historically for describing the pile driving phenomenon starting with Issacs (1931). An exact solution to Issacs' formulation was proposed by Fox (1932) with its practical finite difference formulation applicable for a numerical solution including the hammer-pile-soil model provided by

Smith (1960). The familiar form of the 1-D W.E. modified to accommodate resistance along the pile may be represented as follows:

$$\rho_p \frac{\partial^2 u}{\partial t^2} = E_p \frac{\partial^2 u}{\partial x^2} - f \frac{S_p}{A_p} \tag{5}$$

where:
E_p – modulus of elasticity of the pile
ρ_p – unit density of the pile
f – friction stresses along the pile
S_p – circumference of the pile
A_p – cross-sectional area of the pile
u (x,t) – axial (longitudinal) displacement of infinitesimal pile segment
$c=\sqrt{E_p/\rho_p}$ – one dimensional wave speed propagation

For no external forces (i.e. $f=0$), equation (5) becomes the regular familiar 1-D W.E., which is also a one-dimensional version of equation (4) when assuming that the material, in addition to being elastic and homogeneous, has a prismatic slender shape (i.e. uniform cross-section small in dimension relative to the length of the body assuming to be infinite), and each cross-section must remain plane and parallel while loaded in a manner that will produce a uniform stress distribution throughout each plane.

The assumption of uniaxial stress does not imply uniaxial strain since Poisson's effect produces lateral expansions and contractions (Graff, 1975). In addition, when adding the external forces component to the 1-D W.E. (equation 5 formulation), the soil is assumed to remain stationary so that inertial effects do not influence the frictional (external) resistance, which also must not violate any of the aforementioned assumptions.

These underlying assumptions used for the theoretical description of the pile condition during driving are adequate for most practical purposes. To ensure the validity of the above analysis for open-ended pile penetration, two possible inner soil-pile interactions must be examined; (a) intrusion of soil into the pipe pile during its penetration in an unplugged mode, and (b) pipe pile penetration in a fully plugged mode.

4.2 Unplugged pipe pile penetration

Generally, unplugged piles satisfy the assumptions of material homogeneity and prismatic shape for the pipe. Even a reinforced concrete pile may be represented as a homogeneous pile by using a weighted average for the modulus of elasticity. Furthermore, the loading is such that a uniform stress distribution exists across each plane, neglecting the effects of the friction stresses, which are less than 1% of the propagating stress (Paikowsky, 1989). The soil displacement violates the assumption of stationary soil. However, the damping coefficient often indirectly accounts for the inertial effects of the soil, particularly under hard driving conditions. Under easy driving conditions, the neglect of the soil inertia in the equation of motion (i.e. using the wave equation assuming the resisting forces are stationary) often results with a significant under prediction of the pile capacity. For more details see Hajduk et al., 2000 for soil acceleration due to pile penetration and Paikowsky and Stenersen, 2000 for the performance of dynamic analyses under the conditions of large soil inertia.

During unplugged penetration, the inside and outside friction can be cumulatively represented by one friction stress. Analysis of the dynamic measurements obtained during driving of unplugged, open-ended, large-diameter piles, using the above approach, was presented by Paikowsky (1982). Fig. 9 presents measurements and analysis results of a 60 in (1524 mm) unplugged pipe pile driven with a Menck 2500. The pile length was 216.2 ft (65.9 m) and the penetration was 101.7 ft (31.0 m) with a plug length of 99.7 ft (30.4 m). Fig. 9a shows the measured force and velocity (multiplied by the pile impedance) at the pile's top and the measured force at the pile's tip. The calculated and the measured forces at the top and the tip of the pile are shown in Figs. 9b and c, respectively.

The pile capacity was estimated using a signal matching computer code called TEPWAP. TEPWAP (Paikowsky, 1982) utilizes a procedure similar to the CAPWAP analysis described by Goble et al. (1975). This program allows the input of the measured velocity at the pile top as a function of time, solving equation (5) for a set of parameters describing the soil resistance (dynamic and static) along the pile. Adjustments of the parameters were made until the calculated force at the top matched that measured, as shown in Fig. 9b. Fig. 9c presents the comparison between calculated force at the tip (obtained upon the completion of the above procedure with no other manipulation) to the measured force at the tip. The match between these forces at the tip verifies the validity of the analysis. From the calculated resistance that led to the match in Fig. 9b, the static component acting cumulatively on the inside and outside walls and tip of the pile was predicted to be 2450kips (10.9 MN), compared with 2700kips (12.0 MN) measured in a static load test. The described analysis of pile T-1/B relates to four offshore static load tests of up to 2700kips (12 MN) that were found to be consistently in 90% agreement with the predicted static capacity.

Fig. 10 presents the relations between the measured static capacity to the signal matching predictions where in all the cases the piles clearly penetrated in an unplugged mode. From these analyses and other similar experiences, it can be concluded that when an open-ended pile penetrates in an unplugged mode, a dynamic analysis can be conducted by considering

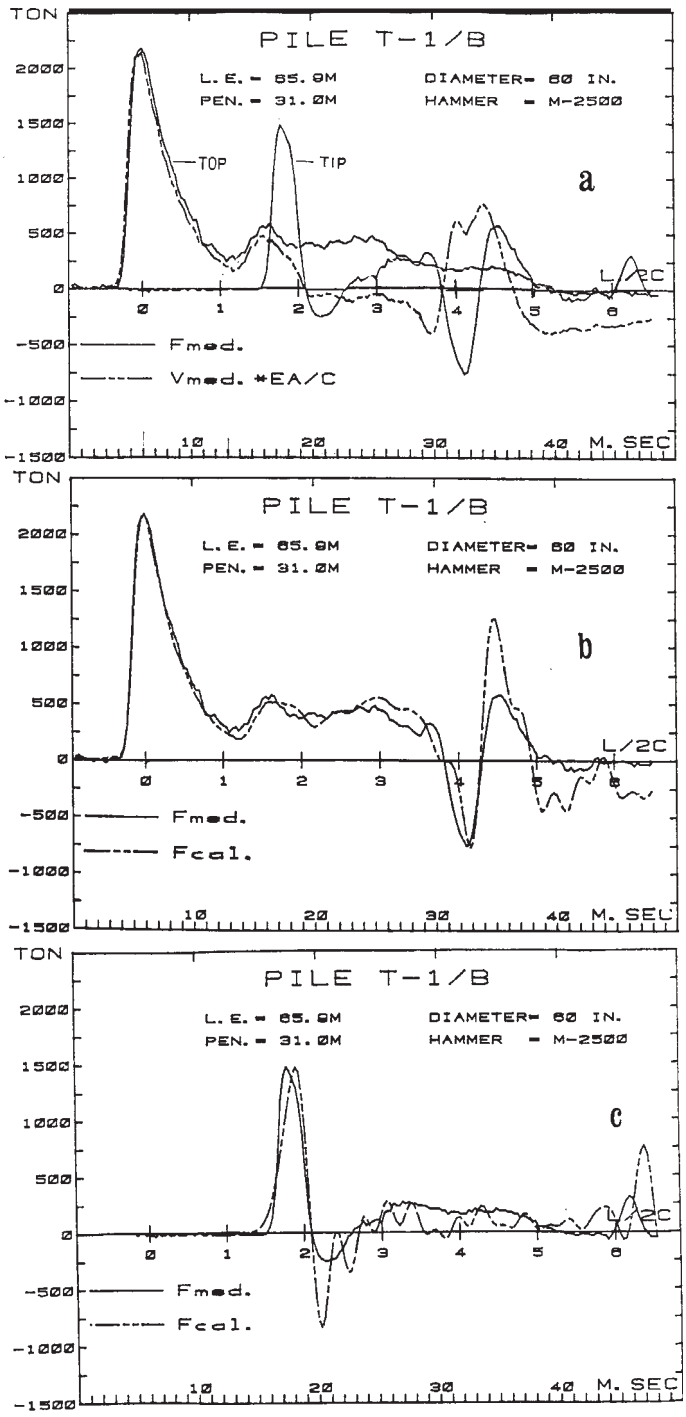

Figure 9. (a) Measurements of force and velocity vs. time for an unplugged pile, (b) Plot of measured force at pile top compared to force obtained from TEPWAP analysis, and (c) Comparison between measure force near tip of pile and calculated force obtained from TEPWAP analysis (referring to measurements at pile top) (Paikowsky, 1982).

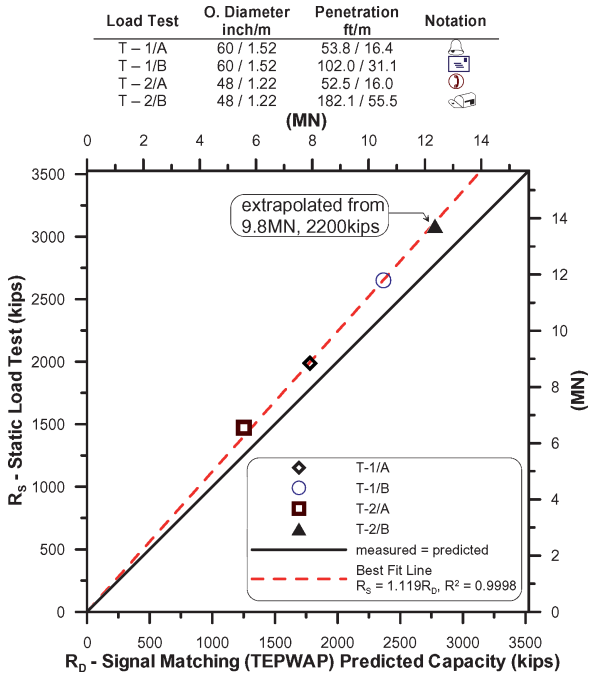

Figure 10. Comparison between signal matching capacity predictions and four offshore static load test results on unplugged open pipe piles in calcareous sand.

only the resultant of the inner and outer wall friction using the common 1-D W.E. solution.

4.3 *Plugged pipe pile penetration*

When a pipe pile becomes fully plugged during penetration, the dynamic conditions differ from those previously described for closed and open-ended unplugged piles.

When a nonhomogeneous pile is subjected to an impact stress, the assumption that a plane parallel cross section remains plane implies strain compatibility, i.e. uniform strain throughout the cross section, and therefore a combined modulus of elasticity can be used (e.g., reinforced concrete pile). However, in a plugged pile only the steel pipe is subjected to the impact. When the propagating stress wave encounters the plug, it is subjected to an abrupt change in the cross section. If full compatibility between the pile and the soil plug is assumed, the problem can be overcome by considering the different impedances of the two sections.

A simple dynamic evaluation of the plug behavior, assuming a rigid soil plug and full compatibility, can be developed as follows. When the soil mass accelerates with the pile wall, the inside shaft friction is given by:

$$f_s = \frac{a_{cc}}{g} \times \frac{\gamma_t \pi B^2/4}{\pi B} = \frac{a_{cc}}{g} \times \gamma_t \times \frac{B}{4} \qquad (6)$$

The pile's acceleration during driving is on the order of a few hundred g's (say $a_{cc} = 200$ g), and therefore the friction is about 1B MN/m^2 (B is the pile diameter in meters). Calculations of friction stresses using (6) for large diameter pipe piles would indicate that such piles can never plug, especially when considering soil softening during pile driving. However, since such piles do plug, the assumption of full compatibility is unlikely. The soil plug, being incompatible, is subjected to radial shear-stress propagation in addition to longitudinal compressive stress. An analysis of this system requires separate consideration of the inertia of the soil plug itself, even though the pile and the plug undergo equal displacement. This complex pile-plug behavior is not consistent with the simplified underlying

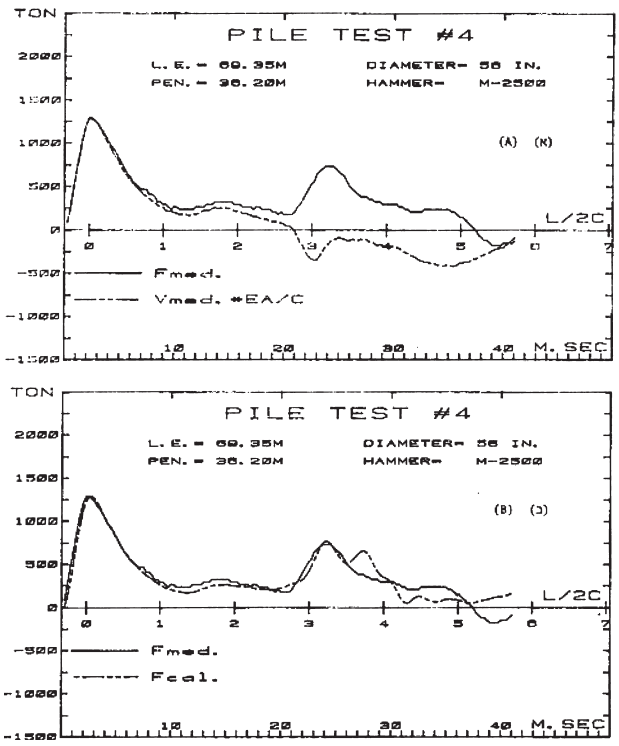

Figure 11. (a) Measurements of force and velocity vs. time for a plugged pile, (b) Plot of measured force at pile top compared to force obtained from TEPWAP analysis (Paikowsky, 1982).

assumptions of (5) so that fully plugged piles cannot be analyzed utilizing the 1-D W.E.

Analysis of the dynamic measurements obtained during driving of an artificially plugged pile (concrete plug, internal annulus) was performed using TEPWAP. Fig. (11) presents a comparison between calculated and measured forces at the top of a 56-inch (1422-mm) plugged pile driven with a Menck 2500. The pile length was 227.5 ft (69.35 m) and the penetration was 118.8 ft (36.20 m) with a plug length of about 98.4 ft (30 m). Even though a reasonable agreement is observed in the signal matching presented in Fig. 11b, the predicted capacity resulting from this analysis was unacceptably low and could not explain the gain in capacity (compared to the unplugged condition), which was indicated by the very high driving resistance observed in the field. Similar results from W.E. analysis were reported by Stevens et al., 1982. Raines et al., (1992) found that analyses of open pipe piles driven in dense saturated sand predicted static pile capacities of approximately 60–70% of the static load test values.

4.4 Intermediate conclusions and earlier solutions

The inner soil in a fully plugged pile exhibits a complex behavior under the dynamic loads of driving. Analyses using the 1-D W.E. fail to model correctly the actual plug-pile interaction, and so do not accurately predict field behavior or explain dynamic measurements.

Several attempts were made to resolve the problem of the dynamic analysis of plugged piles. Heerema and

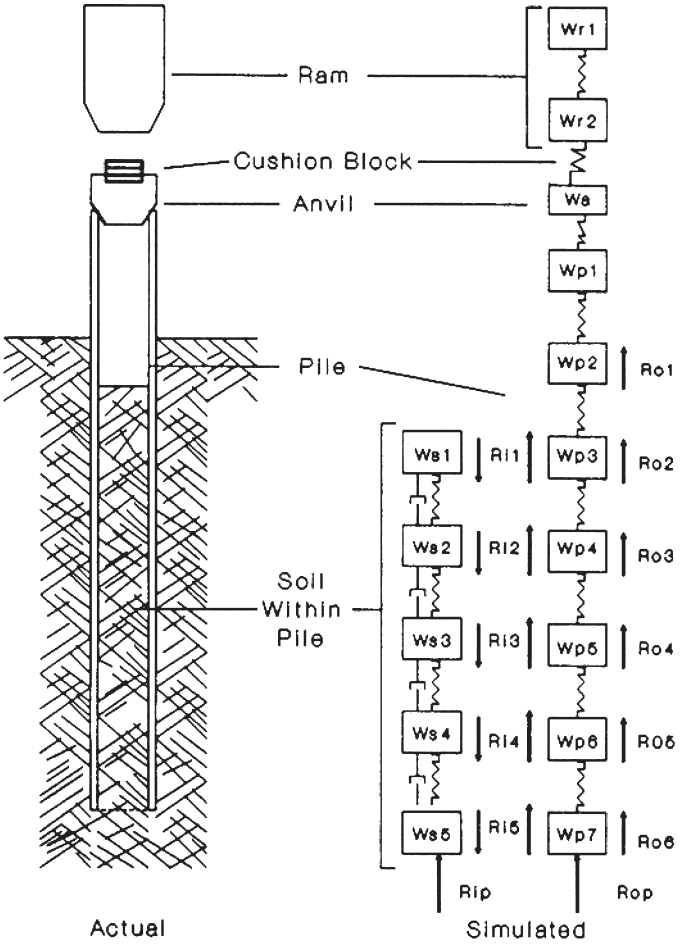

Figure 12. "Pile within a pile" model (Heerema and de Jong, 1980).

de Jong (1980) modeled the inner soil plug as an independent lumped mass-spring system subjected to limited friction induced by the inner pile wall. This pile within a pile system shown in Fig. 12 does not correctly model the actual mechanism as described above and is, therefore, adequate only as long as the pile remains unplugged.

Three dimensional dynamic finite element modeling (e.g., Smith and Chow, 1982; Simons, 1985; Smith et al., 1986) has the potential of solving the problem through a detailed mesh, which allows for both shear and normal stress propagation in the soil plug, as well as the wave traveling in the pipe. However, because of differences in the speed of wave propagation in the two media, the dynamic nature and the relative slippage between the soil and the pile and within the soil mass, the analysis is extremely complex and time consuming, while the simplified meshes and limited codes utilized by the earlier researchers failed to address the complex mechanism of the problem.

Randolph (1987) modified the aforementioned "pile within a pile" analysis of Heerema and de Jong by introducing an extra degree of freedom at each interval soil mode allowing elastic relative displacement between the pile wall and the center of mass of the internal soil. Although being a step in the right direction, the model could not allow sufficient

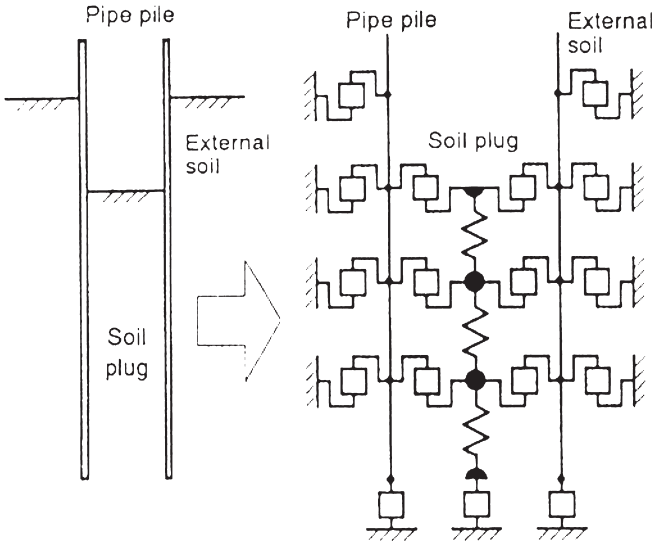

Figure 13. Pile-soil system used by Matsumoto and Takei (1991) to model the plug behavior in driven piles.

consideration for the special plug mechanism, resulting in questionable soil resistances when compared with the measured undrained shear strength of the soil.

Matsumoto and Takei's (1991) expansion of Heerema and de Jong's (1980) and Randolph and Simons' (1986) models is shown in Fig. 13. This model did incorporate the radial shear stress within the soil plug, but failed to address the variation in radial shear stress with the distance from the plug center, since the model remained principally one-dimensional. Hayashi et al. (1994) compared dynamic analysis prediction using the code presented by Matsumoto and Takei (1991) to static load test measurements on open pipe piles driven in mixed soil conditions. Though Hayashi et al. (1994) concluded that for all practical purposes, a reasonable comparison was obtained, none of the static load tests was carried out to failure and the predicted capacities were systematically lower than the maximum loads under which the piles were tested.

The above discussion leads to the conclusion that when an open-ended pile penetrates in a plugged mode, a complex mechanism of pile-plug interaction and independent plug behavior renders the prevailing dynamic pile analysis method invalid.

The above described models tried to address the open pipe pile-plug problem by allowing slippage between the inner soil and the pile, and separately addressing the soil mass and its response via a longitudinal wave motion. None of the models coupled the inner soil radial and longitudinal wave motion and related it to the external one dimensional wave propagation within the pile itself. As such, the solutions which may provide some improvement over the traditional one dimensional wave propagation do not address the fundamental violation of its formulation by the soil plug and hence remain theoretically inadequate to model the physical problem.

5 CONCEPT OF PLUGGED PILE DYNAMIC ANALYIS MODEL

A comprehensive solution needs to address the variation in the radial shear stress with the distance from the plug center along with its longitudinal motion taking place at a different wave speed than the wave in the pile along with a relative displacement between the pile wall and the soil.

The plug was, therefore, modeled separately so that radial wave propagation could be taken into account, as well as compressive wave propagation within the pile and the plug. This enabled simultaneous calculation of inertial forces in each system. The friction developed between the plug and the pile represents a common boundary, thereby ensuring compatibility of forces and, hence, equilibrium between the two systems during driving conditions. This becomes especially important when considering most often encountered partially plugged piles, where the plug periodically breaks free (''slips'') and then moves with the pile wall (''sticks'') as driving proceeds. The radial shear wave traveling through the plug created compressive stress waves acting independently from the compressive stress wave in the pile.

The pile-plug system can be thought of as a cylinder within a pipe. The governing equations of motion for slender elastic cylinders were, therefore, investigated. Refer to Fig. 14 for the generalized representation of the plug within the pile. The depth of the soil outside the pile (embedment) is represented by D. The length and radius of the soil plug inside the pile are represented by L and R, respectively. The two basic modes of stress wave propagation in slender elastic rods are dilational and distortional (Habberstad, 1971). In reference to wave mechanics as it relates to pile driving, dilational waves may be thought of as compression or longitudinal waves, while distortional waves may be thought of as shear waves. As shown in Fig. 14, the shear waves propagate along the radial axis, r, where the positive direction proceeds from the center of the plug to the pile wall. The compressional waves propagate parallel to the plug axis, z, where the

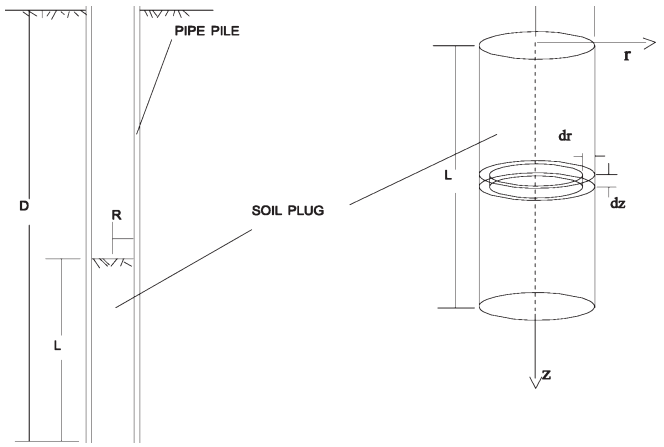

Figure 14. Geometric representation of the pile-plug system as an elastic cylinder within a pipe.

positive direction proceeds from the top to the bottom of the plug. Each plug ring element is represented differentially by the infinitesimal width, dr, in the radial direction and the infinitesimal height, dz, in the longitudinal direction.

Once the basic governing equations were established for slender elastic cylinders in general, boundary conditions specific to the pile-plug system (i.e. soil cylinder within a pipe) were imposed on the equations of motion. Stress wave propagation within the pile was modeled conventionally by using the one-dimensional wave equation from the reasons mentioned earlier and since the shear deformations within the pile are relatively negligible compared to the compressive pile deformations. The shear stress wave propagation in the soil plug must be addressed, since the shear deformations in the soil are relatively large when compared to the compressive deformations in the soil. Thus, the pile is modeled using the one-dimensional wave equation, while the soil plug is modeled with the axi-symmetric equations of motion, hereafter referred to as the axi-symmetric wave equation. This arrangement allows independent stress wave propagation within the two media, which are coupled by the inner friction between the pile wall and the soil plug.

6 AXI-SYMMETRIC WAVE PROPAGATION IN SLENDER ELASTIC CYLINDERS

6.1 General

Axi-symmetric wave propagation was investigated for the plug by obtaining the governing equations of motion for slender elastic cylinders and modifying them to account for the imposed boundary conditions. This led to simplified axi-symmetric equations of motion, which were then differentiated using a finite difference formulation to accommodate the numerical solution.

6.2 The governing equations

The governing equations of motion for slender elastic rods can be reduced to an axi-symmetric formulation (Habberstad, 1971), which is a private case of three-dimensional wave propagation. The equations of motion in an elastic slender rod were obtained by Skalak (1957) (see Bertholf, 1967 and Habberstad, 1971):

$$\frac{\partial^2 u_z}{\partial t^2} = k_1 \times \frac{\partial^2 u_z}{\partial z^2} + k_2 \times \frac{\partial^2 u_r}{\partial r \partial z} + k_2 \times \frac{1}{r} \times \frac{\partial u_r}{\partial z} + k_3 \times \frac{\partial^2 u_z}{\partial r^2} + k_3 \times \frac{1}{r} \times \frac{\partial u_z}{\partial r} \quad (7a)$$

$$\frac{\partial^2 u_r}{\partial t^2} = k_1 \times \frac{\partial^2 u_r}{\partial r^2} + k_1 \times \frac{1}{r} \times \frac{\partial u_r}{\partial r} - k_1 \times \frac{1}{r^2} \times u_r + k_2 \times \frac{\partial^2 u_z}{\partial r \partial z} + k_3 \times \frac{\partial^2 u_r}{\partial z^2} \quad (7b)$$

where:

$$k_1 = \frac{\lambda + 2\mu}{\rho} \quad (8a)$$

$$k_2 = \frac{\lambda + \mu}{\rho} \quad (8b)$$

$$k_3 = \frac{\mu}{\rho} \quad (8c)$$

z = longitudinal coordinate
r = radial coordinate
t = time
u_z = axial (longitudinal) displacement
u_r = radial displacement
ρ = material unit density
μ, λ = Lamé constants

Refer to Fig. 14 for the orientation and geometry. Equations (7a) and (7b) are based on the assumption that there are no torsional and bending waves, which is similar to the assumptions used in the development of the one-dimensional equation of motion. The axial and radial displacements, u_z and u_r, respectively, are differentiated with respect to time - t, and physical domain (location) - using the coordinates z and r. The term ρ is used to represent the material density and the constants λ and μ are known as Lamé constants, which describe the elastic properties of the medium. Both constants may be expressed in terms of Young's modulus, E, and Poisson's ratio, ν, but μ is usually expressed using the shear modulus, G (Graff, 1975). Equations (8) may be rewritten in more familiar terms as:

$$k_1 = {C_d}^2 = \frac{E}{\rho} \times \frac{(1-v)}{(1+v)(1-2v)} = \frac{G}{\rho} \times \frac{2(1-v)}{(1-2v)} \quad (9a)$$

$$k_2 = \frac{E}{\rho} \times \frac{1}{2(1+v)(1-2v)} = \frac{E}{\rho} \times \frac{1}{2(1-v)} \quad (9b)$$

$$k_3 = {C_s}^2 = \frac{G}{\rho} \quad (9c)$$

where

$$G = \frac{E}{2(1+v)} \quad (10)$$

$$ {C_s}^2 = \frac{1-2v}{2(1-v)} \times {C_d}^2 \quad (11)$$

in which C_s and C_d are the shear wave speed and constrained (longitudinal) wave speed, respectively.

The constants k_1, k_2, and k_3 in equations (8) and (9) are used to represent the characteristic properties of the elastic medium. For the soil plug, the constrained wave speed, C_d, is used rather than the longitudinal wave speed, C_l (also known as the elementary bar velocity). This reflects the constrained conditions that exist in the inner soil cylinder due to the surrounding stiffer pile material. These relationships form the basis for developing the equations of motion and their corresponding characteristic properties for axi-symmetric stress wave propagation in the plug system.

7 AXI-SYMMETRIC WAVE PROPAGATION IN THE PILE-PLUG SYSTEM

7.1 Wave motion in the pile-plug system

The modes of wave propagation in the pile-plug system are shown in Fig. 15. In the pile, the stress waves propagate longitudinally at the elementary bar velocity, C_l, while shear propagation, C_s, and constrained longitudinal propagation, C_d, occur in the soil plug. Longitudinal wave propagation begins at the top of the pile due to the impact of the hammer (denoted by point 1). Free wave propagation occurs (point 2) until the wave encounters resistance due to the outer soil mass, which creates reflections (denoted by point 3). The longitudinal wave encounters the soil plug (point 4), where it generates interfacial shear that results with shear waves propagating radially inward towards the center of the plug. These shear waves create vertical displacements within the plug, causing constrained longitudinal waves to propagate up and down the soil plug. Since the speed of wave propagation in the steel is higher than that in the soil (point 5), the longitudinal wave in the pile may have reached the tip and reflected upward, while the constrained and shear waves propagating in the plug may have moved only a fraction of the distance.

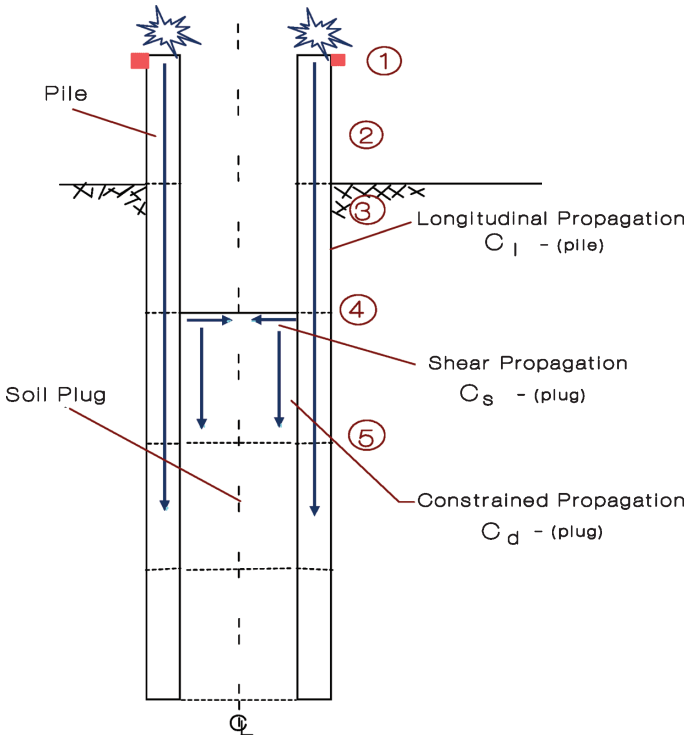

Figure 15. Modes of wave propagation in the pile-plug system.

7.2 Application of boundary conditions to the equations of motion in the plug

It can be assumed that radial displacement, u_r, does not occur within the soil plug for two main reasons:

1. The pile wall prevents meaningful lateral soil displacement (neglecting Poisson's effect) at the pile-plug boundary due to the high stiffness of the steel relative to the soil. Hence, $u_r = 0$ at all $r = R$ locations for all depths ($0 \le z \le L$).
2. Radial displacement cannot occur at the center of the plug due to the plug's axial symmetry. Hence, $u_r = 0$ at all $r = 0$ locations for all depths ($0 \le z \le L$).

It was therefore assumed that radial motion can be neglected throughout the plug leading to $u_r = 0$ for $0 \le r \le R$ and $0 \le z \le L$. As a result, equations (7) reduce to the following simplified forms, respectively:

$$\frac{\partial^2 u_z}{\partial t^2} = k_1 \times \frac{\partial^2 u_z}{\partial z^2} + k_3 \times \frac{\partial^2 u_z}{\partial r^2} + k_3 \times \frac{1}{r} \times \frac{\partial u_z}{\partial r} \tag{12a}$$

$$k_2 \times \frac{\partial^2 u_z}{\partial r \partial z} = 0 \tag{12b}$$

Equation (12b) physically describes the radial variation of the gradient of axial strain. The conditions of equation (12b) were not explicitly imposed as part of the solution, due to the physical modeling requirements of the finite difference formulation. Although, intuitively this route seems reasonable, analytical and/or detailed numerical study were not conducted to confirm this decision. Hence, by substituting equations (9) into equation (12a) the governing equation of motion for the soil plug becomes:

$$\frac{\partial^2 u_z}{\partial t^2} = C_d{}^2 \times \frac{\partial^2 u_z}{\partial z^2} + C_s{}^2 \times \frac{\partial^2 u_z}{\partial r^2} + C_s{}^2 \times \frac{1}{r} \times \frac{\partial u_z}{\partial r} \tag{13}$$

where

u_z – axial displacement of the plug element

$\frac{\partial^2 u_z}{\partial t^2}$ – axial acceleration of the plug element

$\frac{\partial^2 u_z}{\partial z^2}$ – gradient of axial strain within the plug element

$\frac{\partial^2 u_z}{\partial r^2}$ – gradient of shear strain within the plug element

$\frac{\partial u_z}{\partial r}$ – shear strain within the plug element

r – radial coordinate of the plug element

C_d^2 – the square of the constrained wave speed within the soil plug

C_s^2 – the square of the shear wave speed within the soil plug

The detailed resolution of the problem requires a finite difference formulation for solving equation (13) with respect to time and distances (both radially and longitudinally), as well as the integration of the pile's one dimensional formulation with that of the plug. These details are well beyond the scope of the current presentation but can be evaluated via Fig. 16, providing graphically the axis notations and plug dimensions for the differentiation. Each pile element (length Δx) is in contact with several outer plug rings (length Δz) where each ring is in contact with smaller diameter concentric rings all with a cross-section $\Delta z \times \Delta r$ as noted in Fig. 16.

8 EMPIRE PROJECT CASE HISTORY

8.1 The Empire project – overview

Four pipe piles were driven and tested in January, 1975 for a cooperative research study undertaken by Chevron Oil Field Research Company and 13 other participants (Cox and Kraft, 1979, Kraft et al., 1981, Azzouz and Baligh, 1984). The fourth pile, test pile number 4, was selected for the presented analysis. An 18 in (457 mm) diameter steel casing was driven to a depth of 320 ft (97.5 m). The soil within the casing was subsequently cleaned out. A pile 14 inch (35.6 mm) O. D., 0.594 inch (15.1 mm) wall thickness was then driven inside the conductor with a Vulcan O-20 steam hammer (operating at 1/2 stroke) through a stiff, normally consolidated clay with interbedded silt and sand lenses from a depth of 320 to 360 ft (97.5 to 109.7 m) below the ground surface. The casing and pile geometries are provided in Fig. 17 for details.

Dynamic testing was performed on test pile number 4 by Goble (1975). Four CAPWAP analyses were also included in the study. Upon inspection of the dynamic records, it was decided that the pile was partially plugged near the end of driving. The sixteenth blow between penetration from 359 to 360 ft (109.4 to 109.7 m) (or second blow before the break), was selected based on this assumption. The dynamic records containing the force and velocity traces for this blow were digitized from Goble (1975).

8.2 Static load test results

Test pile number 4 was statically loaded in compression to failure four days after the end of driving. One day later, the pile was statically loaded in tension to failure. Approximately one year later (327 days), a second series of compression and tension load tests were performed to evaluate the effect of time on pile capacity and adhesion. The compression test was performed first, followed by a tension test approximately 3-1/2 hours later, followed by another compression test approximately 2-1/2 hours after the tension test. A sequence of cyclic and variable speed static tests were also performed after the compression and tension load tests in the second series. The results of the compression and tension load tests are provided in Table 1 based on Cox and Kraft (1979). Table 1 presents the yield load and average soil adhesion in kips and ksf, respectively, with time interval between tests. Refer to Kraft et al. (1981) and Cox and Kraft (1979) for more details on the test results of test pile number 4.

8.3 Outline of the dynamic analysis

For this study, test pile No. 4 of the Empire Project was analyzed. Initially, standard signal matching TEPWAP analyses (without numerically modeling

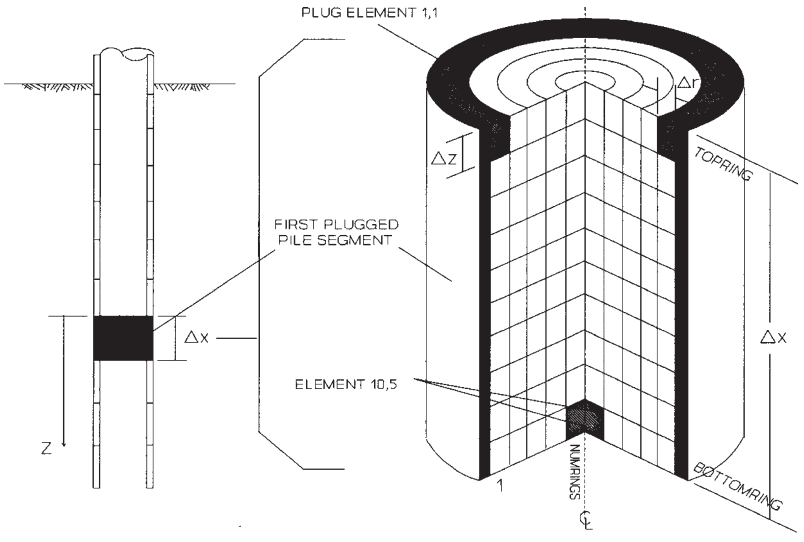

Figure 16. Finite difference representation of the soil plug matrix for the axi-symmetric Wave Equation.

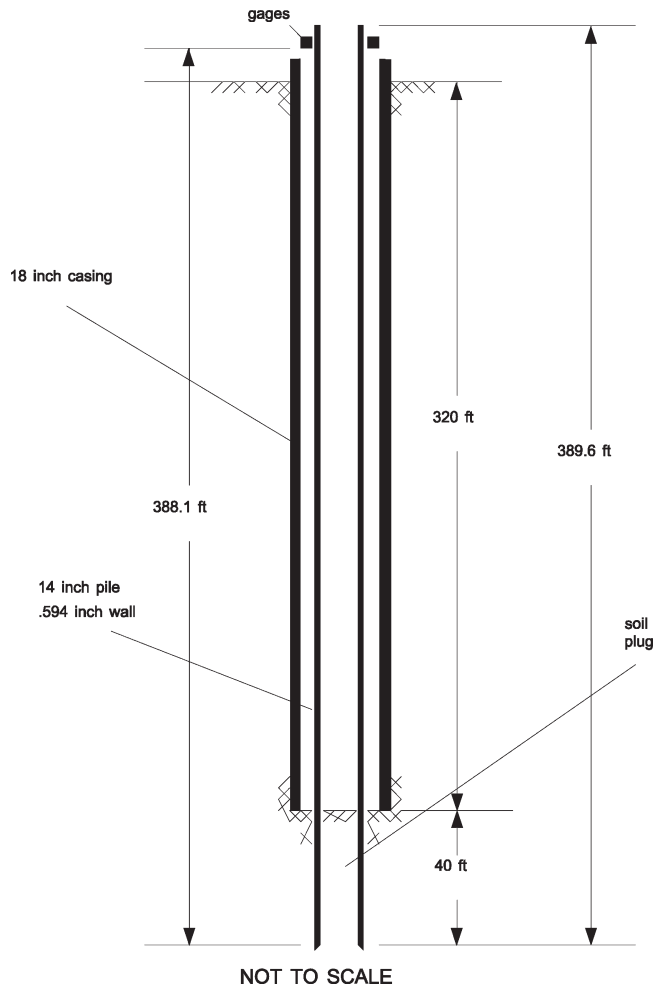

Figure 17. Test pile number four geometry (after Goble, 1975).

Table 1. Empire test pile number 4 load test results

Test Series	Test Mode	Yield Load[1] (kips/kN)	Interpreted[2] Capacity (kips/kN)	Average Soil[3] Adhesion (ksf/kPa)	Time Interval Between Tests
1	Compression	540/2402	480/2135	3.23/155	4 days - 1 hr[4]
	Tension	284/1263	250/1112	2.00/96	24 hrs - 41 min
2	Compression	373/1659	370/1646	2.37/113	327 days
	Tension	290/1290	290/1290	2.04/98	3 hrs - 20 min
	Compression	326/1450	326/1450	2.06/99	2 hrs - 35 min

the plug) were performed followed by PWAP analyses, in which wave motion in the plug was numerically modeled. This was done in order to compare the results of the two and to determine whether the plugging formulations provided better results. The following analyses were performed for the above mentioned blow:

a) TEPWAP (Best Match); Conventional one-dimensional analysis that provided the best force match (CAPWAP analysis results were also available for comparison).
b) TEPWAP (WOP); Conventional one-dimensional analysis, but incorporating the weight of the soil plug (WOP) by lumping it with the weight of the pile.
c) PWAP (Theoretical); Analysis using the axi-symmetric wave equation to model the plug and the one-dimensional wave equation to model the pile as previously discussed. The soil parameters used to model the plug were site specific values based on the Empire clay laboratory results and relevant correlations. The objective of this analysis was to determine if the plugging formulations produced reasonable results when using ‘‘actual’’ soil parameters and, therefore, does not necessarily reflect the best force signal match.
d) PWAP (Best Match); same as the above case ‘c’, but using soil parameters for the plug and the pile that provided the best force match.

All of the above analyses were carried out as class ‘C’ predictions (Lambe, 1973), which are categorized as cases where the actual results (e.g. load tests) are available, but are not known at the time the analysis was performed. For this study, the static load test results were searched for (Cox and Kraft, 1979 and Kraft et al., 1981) and found only after the above analyses were completed. Therefore, the results represent ‘‘true predictions’’ that were not influenced by the outcome of the static load tests.

8.4 Dynamic analyses results

Fig. 18 presents the measured force and velocity signals at the pile top at the end of driving. The best possible match between the force measured to the force calculated using TEPWAP (case ‘a’ section 8.3) is shown in Fig. 19. This analysis resulted in a

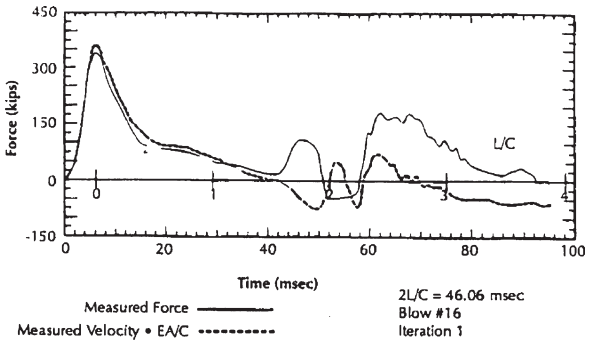

Figure 18. Measured force and measured velocity times the pile impedance (V•EA/C) at the pile top vs. time at the EOD of Empire Site test pile no. 4.

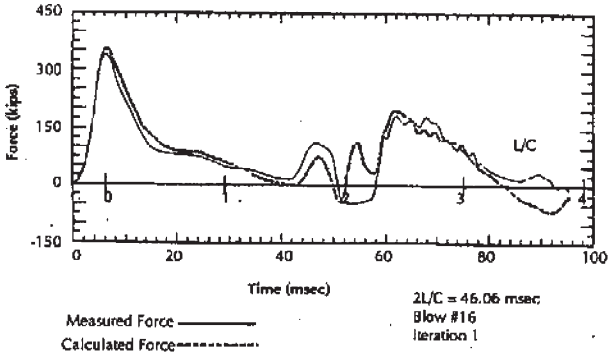

Figure 19. Measured force and force calculated by TEPWAP (best match) at the pile top versus time using the data presented in Fig. 18.

static capacity evaluation of 140kips (0.623 MN). An independent CAPWAP analysis on the same blow showed a similar (poor quality) match as the one presented in Fig. 19 with the same static capacity prediction. Fig. 20 shows TEPWAP best match when the plug mass was lumped together with that of the pile, (case 'b' section 8.3, based on full plugging conditions). Though relatively a very good match was obtained between the calculated and the measured forces; the analysis resulted in a static capacity of 140kips (0.623 MN), identical to that obtained for the wave match in Fig. 19.

Fig. 21 presents the best wave match results of the Plug Wave Analysis Program (PWAP) based on the aforementioned formulation (case 'd' section 8.3). This match does not differ much from that presented in Fig. 20. However, it resulted in a capacity prediction of 396kips (1.761 MN) and a predicted load settlement relation that matches very nicely the two load tests carried out in the field as indicated in Fig. 22.

8.5 Conclusions

Since the physical phenomenon of a driven plugged pipe pile violates the underlying assumptions of the one dimensional WE, analyses based on that formulation lead to erroneous results – even when a very close match between the measured and calculated signals can be obtained. The complex analysis based on the rigorous solution of the plug's equations of motion more accurately models the physical behavior, hence, leads to excellent agreement between the measured and calculated load settlement relations.

The complex analysis methods presented here clearly illustrate the need to question the theories and go back to the original assumptions. The prediction of pile capacity using dynamic measurements requires experience, engineering judgment and a fundamental understanding of the assumptions and methodology.

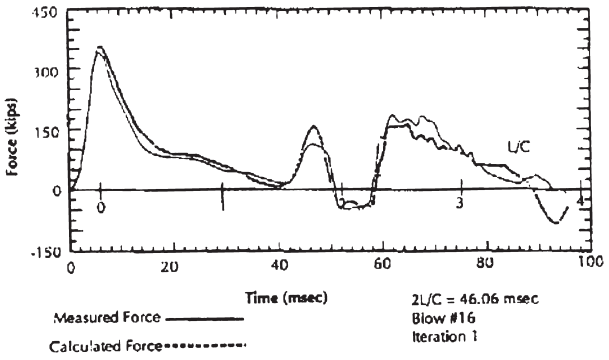

Figure 20. Measured force and force calculated by TEPWAP (lumping the plug's mass together with that of the pile) at the pile top versus time using the data presented in Fig. 18.

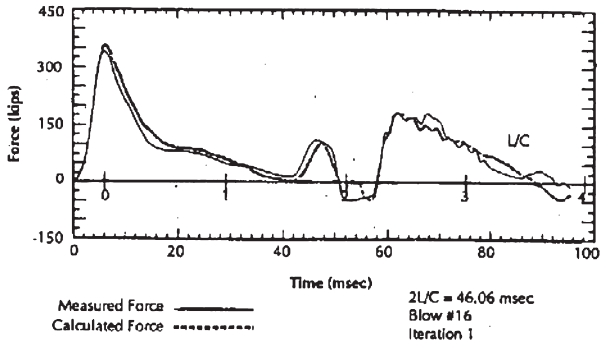

Figure 21. Measured force and force calculated by PWAP (best match) at the pile top versus time using the data presented in Fig. 18.

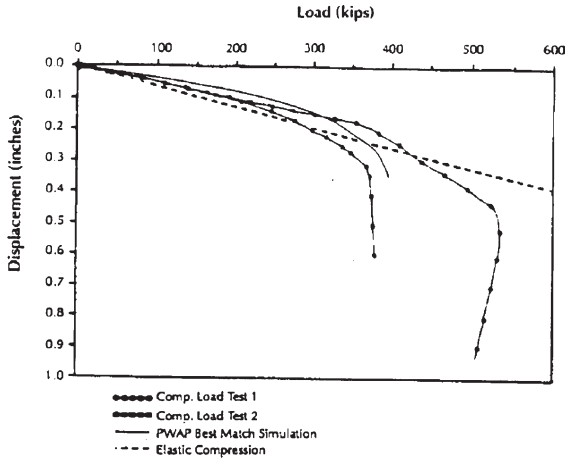

Figure 22. Load test simulation for Empire Site Test Pile No. 4 as obtained from best match PWAP analysis compared to the actual static load tests.

9 SUMMARY AND CONCLUSIONS

Open pipe piles are widely used in marine construction. The soil penetration into the pile can create a soil plug altering the state of pile penetration from a small displacement, ''cookie cutter'', to that of a large displacement, closed ended pipe. The pile plugging can be monitored by the specific recovery ratio referring to the incremental soil plug length change, in relation to the associated incremental pile penetration. As such, piles can become fully plugged at deep penetration without being identified as plugged from the plug length to pile penetration ratio (PLR) alone.

Penetration in a plugged mode increases the zone of pore pressure build up around piles driven in clay and, hence, the time for its dissipation and pile capacity gain. For piles driven in sand, the formation of a solid plug greatly increases the pile capacity and alters the mode of failure under static load. The formation of a plug in an open pile driven in sand is possible via stable passive arching at the lower part of the pile. This complex mechanism creates zones of varied density in the plug associated with the formation and failure of the arches until stable arching conditions are developed.

While driven unplugged, the inner and outer soil resistances can be combined and the dynamic pile penetration can be simulated by the one dimensional

wave equation. Signal matching analyses based on this formulation show good agreement with static load tests, similarly to other small displacement driven piles. When driven plugged or partially plugged, the inner soil plug-pile interaction violates the underlying assumptions of the one dimensional wave equation, leading to erroneous results even when a close match is observed between the measured and calculated signals. A rigorous formulation of the plug's equation of motion accounting for both the shear and longitudinal wave propagation, seems to correctly capture the physical phenomenon. Analysis using a numerical solution for this formulation was proven to provide realistic capacity evaluation much different than that obtained from the one dimensional wave modeling though both presented similar quality signal matching.

The increase in demand (loading) combined with increase in material and construction costs leads to development of induced plugging as a mean of achieving large capacities at shallower depths. Such solutions demand more than ever an adequate dynamic analysis for reliably evaluating their performance. This futuristic trend recently tested could not have been included in this paper but is provided as part of the presentation associated with this manuscript.

ACKNOWLEDGMENTS

The presented material spans research and project experiences since 1979. Many colleagues and students were involved in the different aspects of the manuscript to its various components. The authors would like to mention some of the contributors knowingly missing many others. Late Prof. George Zeitlen exposed the first author to the challenges of offshore open pipe pile design and dynamic measurement analysis. The cooperation with Dr. Frank Rausche of Pile Dynamics over the many years was always rewarding. Prof. Robert Whitman of MIT was a tolerant advisor to the first author, allowing the development of the relations between micro mechanics and sand behavior in the pile plugging problem. This topic was greatly advanced via research support of the Air Force Office of Scientific Research (AFOSR) and the National Science Foundation (NSF). The understanding of pile capacity gain with time was mainly achieved via research support of the Massachusetts Highway Department (MHD). The cooperation and friendship of Mr. Nabil Hourani, the head of the MHD Geotechnical section is greatly appreciated. Mr. Leo Hart and Dr. Edward Hajduk are acknowledged for their dedicated superb work in that area. Last, but not least, the authors are thankful to Ms. Mary Canniff of GTR for her great contribution in putting this manuscript together.

REFERENCES

Azzouz, A.M., and Baligh, M.M. (1984). ''Behavior of Friction Piles in Plastic Empire Clays'', Massachusetts Institute of Technology Report No. R84-14, 3 volumes, Cambridge, MA, September 1984.

Bertholf, L.D. (1967). ''Numerical Solution for Two-Dimensional Elastic Wave Propagation in Finite Bars'', Journal of Applied Mechanics, September, pp. 725–734.

Bransby, P.M., Blair-Fish, P.M., and James, R.G. (1973). ''An Investigation of the Flow of Granular Materials'', Powder Technology 8, pp.197–206.

Cox, W., and Kraft, L. (1979). ''Axial Load Tests on 14-inch Pipe Piles in Clay'', Proceedings of the 11th Offshore Technology Conference, Houston, OTC 3491, pp. 1147–1151.

Fox, E. (1932). ''Stress Phenomena Occurring in Pile Driving'', Engineering Journal, London, Vol. 134.

Goble G.G. (1975). ''A Dynamic Pile Test on Load Test Pile Number 4'', Submitted to the Chevron Deep Axial Pile Research Program, March 6, 1975.

Graff, K.F. (1975). ''Wave Motion in Elastic Solid''s, Ohio State University Press.

Habberstad, J.L. (1971). ''A Two-Dimensional Numerical Solution for Elastic Waves in Variously Configured Rods'', Journal of Applied Mechanics, pp. 62–70.

Hajduk, E.L., Paikowsky, S.G., Hölscher, P., and Barns F. (2000). ''Accelerations of a Driven Pile and the Surrounding Soil'', Proceeding of the Sixth International Conference on the Application of Stress-Wave Theory to Piles, Niyama S. and Beim J. ed., September 11–13, São Paulo, Brazil, pp. 541–561

Hayashi, M., Okamoto, T., Kanai, F., and Matsumoto, T. (1994). ''Predictions of Load-Settlement Relations of Steel Pipe Piles from Dynamic Load Testing'', Proc. 5th International DFI Conference and Exhibition on Piling and Deep Foundations, June 13–15, Bruges, Belgium, Westrade Fairs LTD., pp. 391–397.

Heerema, E., and de Jong, A. (1980). ''An Advanced Wave Equation Computer Program Which Simulates Dynamic Pile Plugging Through A Coupled Mass-Spring System'', Numerical Methods in Offshore Piling, Institution of Civil Engineers, London, pp. 37–42.

Issacs, D. (1931). ''Reinforced Concrete Pile Formula'', Transactions of the Institution of Engineers, Australia, Vol. 12, pp. 312–323.

Kraft, L., Cox, W., and Verner, E. (1981). ''Pile Load Tests; Cyclic Loads and Varying Load Rates'', Journal of Geotechnical Engineering, Proceedings of ASCE, Vol. 107, No GT-1, pp. 1–19.

Lambe, T.W. (1973). ''Predictions in Soil Engineering, 13th Rankine Lecture'', Geotechnique, Vol. 23, No. 2, pp. 149–202.

Matsumoto, T., and Takei, M. (1991). ''Effects of Soil Plug on Behavior of Driven Pipe Piles'', Japanese Society of Soil Mechanics and Foundation Engineering, Soils and Foundations Vol. 31, No. 2, pp. 14–34.

Paikowsky, S.G. (1982). ''Use of Dynamic Measurements to Predict Pile Capacity under Local Conditions'', M.Sc. Thesis, Technion, Israel Institute of Technology, July 1982.

Paikowsky, S.G. (1989). ''A Static Evaluation of Soil Plug Behavior with Application to the Pile Plugging Problem'', D.Sc. Dissertation, M.I.T., Cambridge, MA.

Paikowsky, S.G., Whitman, R.V., and Baligh, M.M. (1989). ''A new Look at the Phenomenon of Offshore Pile Plugging'' Marine Geotechnology, Taylor & Francis, Vol. 8, pp. 213–230.

Paikowsky, S.G. (1990). ''The Mechanism of Pile Plugging in Sand'' Proceedings 22nd Annual Offshore Technology Conference, Houston, Texas, May 7–10, pp. 593–604.

Paikowsky, S.G., and Whitman, R.V. (1990). ''The effects of plugging on pile performance and design'' Canadian Geotechnical Journal, Vol.27, pp. 429–440.
Paikowsky, S.G., LaBelle, V.A., and Mynampaty, R.N. (1995). ''Static and Dynamic Time Dependent Pile Behavior'', Research Report submitted to the Massachusetts Highway Department, October.
Paikowsky, S.G., and Hart, L.J. (2000). ''Development and Field Testing of Multiple Deployment Model Pile''; Research Report submitted to the Massachusetts Highway Department and the FHWA, March 1998, FHWA Publication No. FHWA-RD-99-194, 284pp
Paikowsky, S.G., and Stenersen, K.L. (2000). ''The Performance of the Dynamic Methods, their Controlling Parameters and Deep Foundation Specifications'', Keynote lecture in the Proceeding of the Sixth International Conference on the Application of Stress-Wave Theory to Piles, Niyama S. and Beim J. ed., September 11–13, São Paulo, Brazil, Balkema, pp. 281–304.
Paikowsky S.G., and Tien, S.H. (2002). ''Experimental Examination of the Arching Mechanism on the Micro Level'', 3rd Int. DEM Conference, Santa Fe, New Mexico September 23–25, 2002, Cook B.K. and Jensen R.P. edt, ASCE Geotechnical Special Publication No. 117, pp. 222–228.
Paikowsky, S.G., Rolwes, L.E., and Tien, S.H. (2003). ''Visualization and Measurements of Stresses Around a Trap Door'', Proceedings of Soil and Rock America (SARA) 2003, 12th Pan-American Conference on Soil Mechanics and Geotechnical Engineering and the 39th U.S. Rock Mechanics Symposium. MIT, Cambridge, MA, June 22–26, 2003, VGE Pub. Culligan, Einstein and Whittle editors, Vol. 1, pp. 1171–1177.
Paikowsky, S.G., and Hajduk, E.L. (2006). ''Full Scale Field Testing Examination of Pile Capacity Gain with Time'', Research Report submitted to the Massachusetts Highway Department, summer 2006.
Perry, M.G., and Handley, M.F. (1967). ''The Dynamic Arch in Free-Flowing Granular Material Discharging from a Model Hopper'', Trans. Inst. Chem. Engineers, Vol. 45, T367–T371.
Raines, R., Ugaz, O., and O'neill, M. (1992). ''Driving Characteristics of Open-Toe Piles in Dense Sand'', Journal of Geotechnical Engineering, American Society of Civil Engineers.
Randolph, M. (1987). ''Modelling of the Soil Plug Response During Pile Driving'', 9th Southeast Asian Geotechnical Conference, Bangkok, Thailand, pp. 1–14.
Skalak, R. (1957). ''Longitudinal Impact of a Semi-Infinite Circular Elastic Bar'', Journal of Applied Mechanics, Vol. 24, Transactions of ASME, Vol. 79, pp. 59–64.
Smith, E. (1960). ''Pile Driving Analysis by the Wave Equation'', Journal of the Soil Mechanics and Foundation Division, ASCE, Vol. 86, Part 1, pp. 35–61.
Smith, I., and Chow, Y. (1982). ''Three Dimensional Analysis of Pile Drivability'', Proceedings 2nd International Conference on Numerical Methods in Offshore Piling, Austin, pp. 1–19.
Smith, I., To, P., and Willson, S. (1986). ''Plugging of Pipe Piles'', Numerical Methods in Offshore Piling, 3rd International Conference, Nantes, France, pp. 53–73.
Tien, S.H., and Paikowsky, S.G. (2001). ''The Arching Mechanism on the Micro level Utilizing Photoelastic Particles'', Fourth international Conference on Analysis of discontinuous Deformation, N. Bićanić edt., June 6–8, 2001, Glasgow, Scotland, UK, pp. 317–336.
Timoshenko, S.P., and Goodier, J.N. (1970). ''Theory of Elasticity'', third edition, McGraw Hill, pp. 567.

